IEEE Access
Multidisciplinary ⋮ Rapid Review ⋮ Open Access Journal

Received January 8, 2021, accepted January 13, 2021, date of publication January 21, 2021, date of current version February 2, 2021.

Digital Object Identifier 10.1109/ACCESS.2021.3053394

Design, Analysis, and Experiment on High-Performance Orbital Angular Momentum Beam Based on 1-Bit Programmable Metasurface

ZIYANG WANG[1,2], (Member, IEEE), XIAOTIAN PAN[2], FAN YANG[2], (Fellow, IEEE), SHENHENG XU[2], (Member, IEEE), MAOKUN LI[2], (Member, IEEE), AND DONGLIN SU[1,3], (Senior Member, IEEE)

[1]Research Institute for Frontier Science, Beihang University, Beijing 100191, China
[2]Department of Electronic Engineering, Tsinghua University, Beijing 100086, China
[3]School of Electronic and Information Engineering, Beihang University, Beijing 100191, China

Corresponding author: Fan Yang (fan_yang@tsinghua.edu.cn)

This work was supported in part by the National Key Research and Development Program of China under Grant 2017YFA0700201, and in part by the China Postdoctoral Science Foundation under Grant 2019M650677, and in part by Tencent Foundation through the XPLORER PRIZE.

ABSTRACT In this study, a high-performance orbital angular momentum (OAM) beam is designed, analyzed and experimented using a 1-bit programmable metasurface. OAM as a novel technology is investigated systematically in this paper. Moreover, this study is motivated by the application requirements of real-time controllable communication. The proposed programmable metasurface comprises 1-bit phase modulation units with only two phase states, which is evolved from an electromagnetic surface composed of 360° continuous phase units based on the principle of 1-bit phase quantization. First, the necessity and feasibility of developing the OAM beam based on 1-bit programmable metasurface are studied. Then, qualitative analysis of OAM beams is conducted on different OAM modes and phase modulation elements. Next, the quantitative indexes of OAM beams such as the peak gain in far-field, the divergence angle of main lobe, and circumferential symmetry in azimuth planes are systematically analyzed through a survey of key factors. It is noteworthy that this analysis provides a powerful research basis to achieve an excellent OAM beam with the adjustable function. Thereafter, an active reflective programmable metasurface with 48×48 elements is fabricated to verify the feasibility of developing an OAM beam using a 1-bit element. The experimental and simulation results are in good agreement. Furthermore, a high gain OAM beam with a narrow divergence angle is realized by using the large-scale 1-bit programmable metasurface. Notably, a high-gain beam and an OAM beam can be both generated and can converted into each other, which lays the foundation to achieve the OAM beam with the function of real time dynamic control in future.

INDEX TERMS High-performance orbital angular momentum (OAM) beam, 1-bit programmable metasurface, real time dynamic control.

I. INTRODUCTION

Orbital angular momentum (OAM) carried by photons [1] in optical vortices was discovered in 1992. In essence, a light beam as a type of electromagnetic wave has two attributes: energy and momentum. Furthermore, angular momentum includes spin angular momentum (SAM) determined by polarization and OAM determined by spatial distribution of light field, and these are two basic and important concepts in classical physics. On the one hand, SAM has three states: $S = -1$, $S = 0$ and $S = -1$, which correspond to right-hand circular polarization, linear polarization and left-hand circular polarization, respectively. On the other hand, the state of OAM is determined by the topological charge of l. Because of its novel characteristics, OAM is used in optical fields such as microscopy [2], quantum information technologies [3-5], super-resolution imaging [6] and others [7]. Thereafter, OAM has shown great potential in the microwave field in wireless

The associate editor coordinating the review of this manuscript and approving it for publication was Lin Peng.

communications [8]. It has gradually become a hotspot in radio frequency applications. OAM may be useful in improving the channel capacity [9], [10] to meet the shortage in spectrum resources and the rigid demand for system capacity owing to the additional modulated freedom of the helical phase compared with the traditional plane wave.

Various methods are attempted to design and implement OAM beams in microwave bands. A helical phase plate using all-dielectric materials [11]–[14] is designed to achieve the OAM radiation as a direct solution. Thereafter, methods for the design of OAM can be divided into spiral parabolic [15]–[17] and circular-phased array [18], [19] antennas. Artificial electromagnetic material has become an active topic in academia and industry because it can flexibly control the amplitude, phase and polarization of reflected and transmitted waves. Based on the use of the metamaterial, various novel microwave devices have been designed and applied, such as reflectarray [20], transmitarray [21], polarization converter [22], Fabry-Perot antenna [23], particularly after the concept of metasurface (MS) has been proposed. In addition, with the development of the universal theory on surface electromagnetics, the application of metasurface is a great step forward in current microwave and RF domain [24]. Metasurface has many distinct advantages as an important generator or modulator of electromagnetic waves, which are also applied to the design of OAM beams [25]–[27], [37], such as a reflective metasurface [25], anisotropic frequency selective surface (FSS) [26] and anisotropic holographic metasurface (HMS) [27].

However, the reflective or transmissive elements for OAM beams in most published studies were achieved by using cells with 360° full-phase coverage [28], [29], which to an extent increases the structural complexity of the phase modulation unit. In reference [28], a high-gain OAM beam is generated by using a transmission metasurface, and the transmission element with the shape of the British ''Union Jack'' is designed, which consisted of four layers of metal and three layers of medium. In addition, a five-layer spiral phase plate cell [29] for 360° coverage is used to generate an OAM beam at 60 GHz. Therefore, the processing cost and design difficulty of the surface for an OAM beam with an excellent vortex performance are increased. The introduction of coding metasurface [30-32] reduces the design requirement for cell structure (layers) because of the limited discrete phase state. Thus, the phase modulation cell does not need to meet the full coverage of the 360° phase range strictly, such as only two states in the design of a 1-bit element, and the difference between two phase states should be satisfied at approximately 180°. More importantly, the design of 1-bit metasurface for OAM provides a reliable theoretical basis for the subsequent design of an adjustable OAM beam. The active programmable metasurface [33]–[36] based on a 1-bit reconfigurable element can achieve the real-time and dynamic adjustable function. However, few reports [38], [39] are available on OAM beams by using the 1-bit active programmable metasurface.

In this study, the necessity and feasibility of realizing the OAM beam based on 1-bit phase modulation units are verified theoretically. The effects of key parameters on the OAM performance are quantitatively analyzed and systematically summarized. The systematic elaboration of the divergence angle of the main lobe, maximum gain in far field and the fluctuation gain is presented, which are affected by the number of modes, 1-bit phase quantization and number of cells. Based on the preceding analysis and summary, a large-scale 1-bit active programmable metasurface is utilized to achieve the high-performance OAM beam. Data show that the experimental results are in good agreement with the simulation ones. Moreover, a high-gain beam and an OAM beam with a mode of $l = 1$ are realized using the proposed 1-bit programmable metasurface. Furthermore, these two beams can be converted to each other, which is rare among articles published in the same category of metasurface; it also proves that the OAM beam can be obtained using a 1-bit phase element. In addition, the proposed OAM beam has an excellent vortex performance with a high gain of approximately 26.3 dBi and the main lobe has a narrow divergence angle of approximately 1.8°. Thus, the high-performance OAM beam is beneficial to increase the OAM-based communication distance in accordance with the quantitative conclusions summarized in the previous section.

II. ANALYSIS AND DESIGN

Schematic views for both the high-gain beam and OAM beam are presented in Figs. 1(a) and (b), respectively. Arbitrary switching between the high-gain beam and the OAM beam can be achieved based on this proposed 1-bit active programmable metasurface, while only the phase distribution needs to be changed. Therefore, the feasibility of the scheme for the OAM beam should be verified to guide future high-performance adjustable or controllable design by comparing two types of numerical calculation results based on MATLAB software. The selection and design of the 1-bit phase element to analysis the feasibility of OAM beam are presented in this section. Detailed and analytical procedures are described in the following.

A. 1-BIT ELEMENT SELECTION

Firstly, a periodic 1-bit element should be selected to verify the feasibility of the design. Two types of 1-bit programmable element exist: passive 1-bit element with a fixed phase and active reconfigurable 1-bit element. As the full-wave simulation of array by using active reconfigurable 1-bit elements requires considerable time, a fixed-phase 1-bit cell is selected for simplify the calculation and simulation to analysis in this section. And the selected periodic unit should be as simple as possible. In addition, it needs to satisfy the following conditions as far as possible. Firstly, the element of phase should cover approximately 360° because a comparison of the effects for OAM generation by using a 1-bit modulation element and a 360° all-phase unit should be presented. Then, as much energy as possible should be

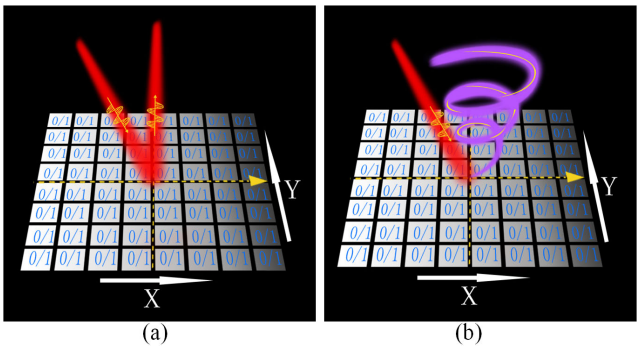

FIGURE 1. Sketch graph of the proposed 1-bit programmable metasurface, (a) for high-gain beam for mode of $l = 0$ and (b) for OAM beam for mode of $l = 1$.

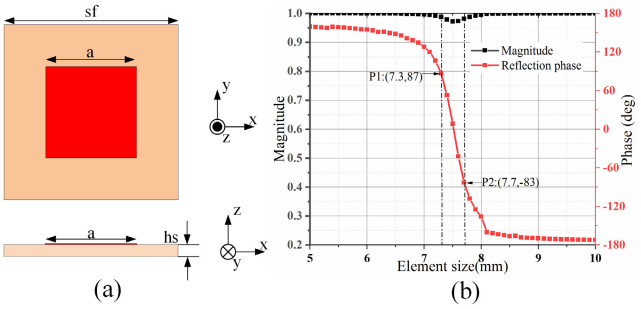

FIGURE 2. (a) Geometrical construction of period unit for 1-bit programmable metasurface. (b) Magnitude and phase response curves with respect to element size.

reflected or transmitted. To sum up the above points, a reflective patch cell is adopted in this section. The configuration of the periodic element is presented in Fig. 2(a). As shown in Fig. 2(b), phase and magnitude responses for different element sizes are also shown. The element is realized by using Taconic TLY substrate because of low cost and minimal loss. The thickness of the dielectric plate is approximately 0.51 mm at 12.5 GHz.

To verify the feasibility of generating of OAM beams by using only two states, the 1-bit element should be selected based on the 360° cell. According to the mechanism of 1-bit phase quantization, two qualified phase points for 1-bit is obtained. As shown in Fig. 2(b), when the length of the element size is equal to 7.3 mm, the phase of the unit is approximately 87°. Another point at roughly 7.7 mm is selected, and the reflection phase is floating at -83°. P1 and P2 represent two states, namely, "0" and "1", respectively. Therefore, a non-reconfigurable 1-bit element with two phase states is achieved.

Thereafter, a numerical simulation and analysis model by using the lossy element mentioned in Fig. 2 is established to investigate the feasibility of achieving OAM beams by using the 1-bit programmable metasurface. As shown in Fig. 3, the OAM reflectarray system consists of a metasurface and a feed. The metasurface consists of periodic cells with unequal dimensions representing different phase information. And the feed that illuminates the electromagnetic metasurface is fixed at a certain height above the metasurface.

B. APERTURE SCATTERING ANALYSIS

An incident wave is emitted from the feed and exposed to each unit of the electromagnetic surface along different paths. Phase modulation and compensation occur through the metasurface. Thus, an OAM beam with a certain beam direction is generated in free space, as shown in Fig. 3. Considering the metasurface, which is composed of M × N period elements illuminated by the source. Moreover, the compensation phase on the surface for OAM can be calculated from Eq. (1) with a different mode. While, k is the propagation constant, r_{fmn} is the positon vector from the feed to element, r_{mn} is the positon vector from the center to element, u_0 is the desire output direction of the OAM beam, and Φ_{mn} is the azimuth at each cell. Furthermore, the element phase for a 1-bit programmable metasurface is selected based on the mechanism of 1-bit phase quantization, as shown in Eq. (2). Therefore, a 1-bit metasurface with only two states of phase is obtained. Hence, the scattered electric fields from the metasurface in an arbitrary direction can be calculated from Eq. (3) based on array theory. In this equation, A_{mn} is the amplitude excited on each cell, and it can be computed by Eq. (4), therefore the electric field at any point in 3D space has been obtained. In which the radiation pattern on feed and patches are expressed on the basis of an approximate cosine mode. In addition, EP is the pattern of patch element, FP is the feed pattern, and Γ_{mn} is the magnitude of the practice element which can be obtained in Fig. 2.

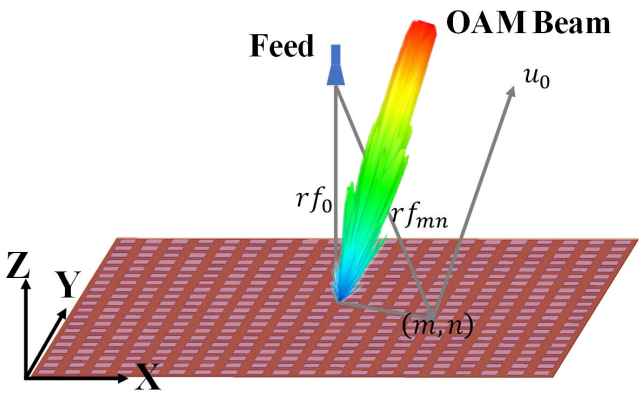

FIGURE 3. Schematic diagram of the 1-bit programmable metasurface for OAM beam.

Based on the mechanism introduced, two numerical models are established by using the mathematical software MATLAB. One of them is a continuous electromagnetic surface realized by 360° phase units, and another is a 1-bit programmable metasurface with only two states of "0" and "1," respectively. Numerical calculation results based on different modulation elements are shown in Figs. 4 (a-h). The compensation phase for each element by using the practical 360° phase element is presented in Fig. 4 (a). Then, the 3D radiation pattern and corresponding 2D radiation patterns in XOZ/YOZ plane are also shown in Fig. 4 (b-d), respectively. Thereafter, the simulated data by using the 1-bit

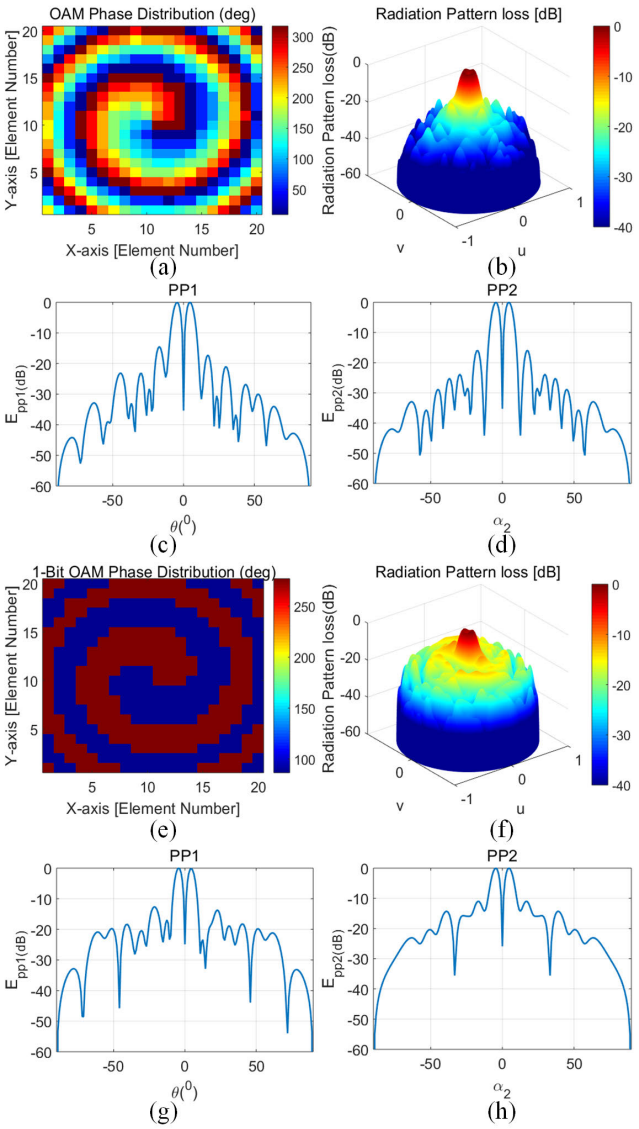

FIGURE 4. Numerical simulation results for mode of *l*= 1 OAM beam using 360° continuous phase element: (a) compensation phase distribution for elements, (b) far-field 3D radiation pattern, (c) 2D pattern in XOZ plane, and (d) 2D pattern in YOZ plane. Numerical simulation results for mode of *l*= 1 OAM beam using 1-bit phase element: (e) compensation phase distribution for elements, (f) far-field 3D radiation pattern, (g) 2D pattern in XOZ plane and (h) 2D pattern in YOZ plane.

phase element for OAM beam with the mode of $l = 1$ are also presented in Figs. 4 (e-h). Only two states are used on the compensation phase distribution for each element, as shown in Fig. 4 (e). Moreover, a deep null exists in the boresight direction in 3D radiation pattern and 2D radiation patterns, XOZ/YOZ planes, as shown in Fig. 4 (f-h). The OAM beam can be obtained by using the proposed 1-bit metasurface. Therefore, this study lays a foundation for the realization of the OAM beam by an active 1-bit programmable metasurface in future.

$$\varphi(m,n)_{OAM} = k \times r_{fmn} - k \times r_{mn} \times u_0 + \Delta\varphi + l \times \Phi_{mn} \quad \text{while } l = 0, \pm1, \pm2, \ldots \tag{1}$$

$$\varphi_{1bitOAM} = \begin{cases} 0, & -\frac{\pi}{2} < \varphi(m,n)_{OAM} < \frac{\pi}{2} or \varphi(m,n)_{OAM} = \pm\frac{\pi}{2} \\ \pi, & -\pi < \varphi(m,n)_{OAM} < -\frac{\pi}{2} or \frac{\pi}{2} < \varphi(m,n)_{OAM} < \pi \end{cases} \tag{2}$$

$$E(\theta,\varphi) = \overset{qe}{\cos\theta} \sum_{m=1}^{M}\sum_{n=1}^{N} A_{mn} e^{(-jkr_{fmn} + j\varphi_{1bitOAM} + jkr_{mn}u)} \tag{3}$$

$$A_{mn} = \frac{FP \times EP \times |\Gamma_{mn}|}{r_{fmn}} \tag{4}$$

III. SYSTEMATIC PERFORMANCE STUDY OF OAM BEAM

No systematic and quantitative study on OAM beam performance has been published, and most studies were focused on OAM phenomena. Therefore, to quantify the effect of OAM performance, certain key parameters are studied, such as 1-bit quantization of element, number of OAM modes and number of cells, which greatly influence the radiation performance of the OAM beams. Furthermore, some quantitative laws on the maximum gain and divergence angle of the main lobe are summarized to improve the OAM performance to guide future high-performance adjustable or controllable design.

Qualitative analysis and quantitative contrast of OAM beams with different models are presented. In the simulation analysis on this section, the aforementioned passive fixed-phase 1-bit element is still used to save time and computer resources.

A. QUALITATIVE ANALYSIS OF OAM BEAMS WITH DIFFERENT MODELS

Six simulation models are established by using the full-wave simulation software HFSS. Feed is located at the center of the reflectarray away from the metasurface in all simulation models. As shown in Fig. 5, the simulated data for far and near fields are presented with different OAM mode combinations working at 12.5 GHz. Six models correspond to six arrays. Array 1 is the reflectarray (RA) for a high-gain beam with mode of $l = 0$. Simulated results of Array 1 are presented in the first column, as shown in Figs. 5 (a), (f), (k) and (p).

1) ELEMENT PHASE QUANTIZATION, 360° FULL-COVERAGE PHASE OR 1-BIT PHASE

Array 2 is the RA for OAM with the mode of $l = 1$ by using the 360° continuous phase element. By which the size of the selected reflective element are equally spaced from 1 mm to 10 mm with an interval of 0.1 mm, and about 91 points are used to represent the 360° continuous phase element. Array 3 is the RA with the mode of $l = 1$ by using the 1-bit phase element. In the second column in Fig. 5 (b), (g), (l) and (q), the far field and near field of Array 2 for the OAM beam are shown. Then, the results on Array 3 for OAM-generation are shown in Fig. 5 (c), (h), (m) and (r) in the third column.

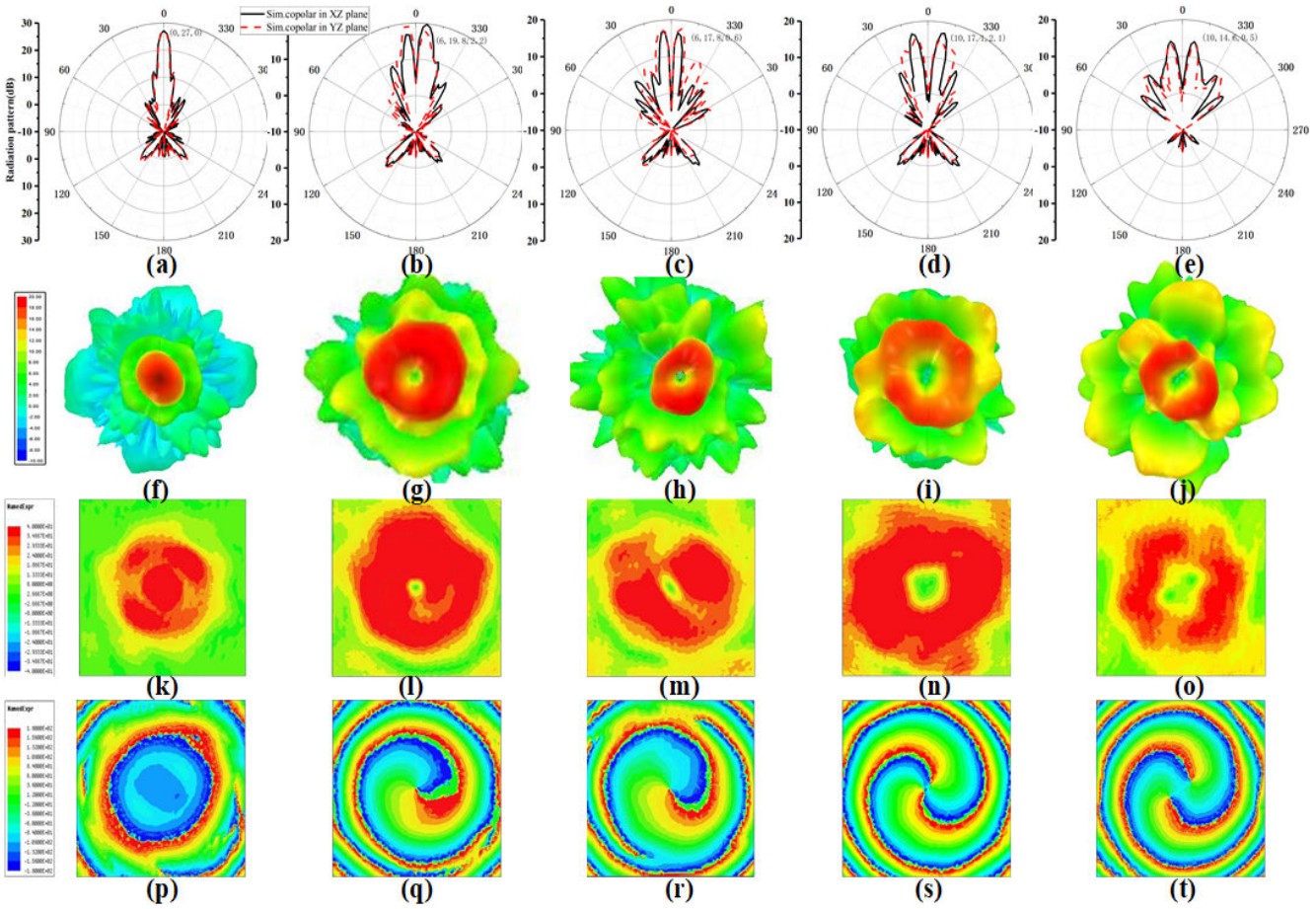

FIGURE 5. Simulation of far-field 2D radiation patterns for OAM beams in XOZ and YOZ planes in the first row: (a) Array 1, (b) Array 2, (c) Array 3, (d) Array 4 and (e) Array 5. Simulation far-field 3D radiation patterns for OAM beams in the second row: (f) Array 1, (g) Array 2, (h) Array 3, (i) Array 4 and (j) Array 5. Simulated magnitude distributions of e-field in near field on XOY plane with distance of 40 wavelengths above the metasurface: (k) Array 1, (l) Array 2, (m) Array 3, (n) Array 4 and (o) Array 5. Simulated phase distributions of e-field in near field on XOY plane with distance of 40 wavelengths above the metasurface: (p) Array 1, (q) Array 2, (r) Array 3, (s) Array 4 and (t) Array 5.

It is clear that the OAM phenomenon is realized, moreover the performance for phase and magnitude distribution in near field and the pattern in far-filed are perfect comparing the array 2 with array 3 only the phase element changing. Which further verifies the conclusion of the numerical simulation in the previous section. Therefore, the feasibility of the 1-bit element to the realization of the OAM beam is confirmed.

Similarly, for mode 2, the case of two different phase modulation units is analyzed. The simulated data for Arrays 4 and 5 are respectively shown in columns 4 and 5 in Fig. 5. Array 4 is the RA with the mode of $l = 2$ by using the 360° phase element, and Array 5 is the RA with the mode of $l = 2$ by using the 1-bit phase element. From the simulated data about Arrays 4 and 5, the same conclusion that the OAM beam can be obtained by using the 1-bit phase element can be reached.

2) MODE $L = 1$ OR $L = 2$

To investigate the effects of different modes by using the 1-bit phase element on the performance of OAM beams, Arrays 3 and 5 are compared. The mode of Array 3 is $l = 1$, while the mode of Array 5 is $l = 2$ with other conditions remaining the same. From the results of a two-dimensional pattern of Arrays 3 and 5 as shown in Figs. 5 (c) and (e), respectively, the pattern of Array 5 is worse than that of Array 3 when the mode increases. The same conclusion can be reached comparing the Array 2 with Array 4 using the 360° phase element. Therefore, certain improvement measures need to be adopted. In addition, the quantitative comparisons should be presented to measure the extent of deterioration.

3) NUMBER OF UNITS: 20 × 20 OR 40 × 40

The simulation data of Array 5 in Fig. 5 (e) shows that a significant deterioration of 2D pattern for Array 5 has occurred. Array 6, with the number of elements 40 × 40, is simulated by using the 1-bit phase element, as the mode is equals to 2. The simulated results for Array 6 are not shown in Fig. 5 because of large size, while the date are counted in Table 1.

2D radiation patterns in the XOZ and YOZ planes for OAM beams are obtained successfully with different cases in the first row in the following order: Arrays 1, 2, 3, 4 and 5. Then, far-field 3D radiation patterns for OAM beams with different situations are also presented in the second row. Next, simulated magnitude patterns of selected OAM mode

in the near field are also displayed in the third row. And the magnitude distributions for OAM carrying are doughnut shaped, and zero point occur in the middle of patterns whether it is generated by 360° phase element or 1-bit element, which is the magnitude features for OAM-carrying in the near field. In addition, the twisted-phase distributions of OAM beams with different states are successfully realized as shown in the fourth row of Fig. 5. Moreover, the change from red to blue color corresponds to the phase variation of 360°.Therefore, the OAM beams with different modes using 1-bit phase element are achieved as shown in Fig. 5.

B. QUANTITATIVE ANALYSIS OF OAM BEAMS

Then, quantitative analyzation for OAM beams should be performed to measure the extent of deterioration. And the performance comparison of OAM beams under different conditions is quantitatively analyzed as shown in Table 1. Thereafter, quantitative indicators for OAM beams are provided in detailed at the following list.

1) THE GAIN IN FAR-FIELD

The information for Array 1 with a high-gain beam are shown in the second row at Table 1. Meanwhile, the indicators corresponding to Arrays 2, 3, 4 and 5 are shown in the third, fourth, fifth and sixth rows. While, the results for Array 6 are for the large-scale array with mode of $l = 2$ by using the 1-bit phase element. In addition, parameters for different arrays are shown in the second column, with different OAM modes, phase elements and array sizes.

Firstly, the gains as the most important index of antenna far-field radiation performance are investigated for OAM beams. The gain in Table 1 is the maximum peak gain in all directions of observation. In the third column, the gain of Array 1 without OAM carrying is approximately 27 dBi. The gain decreases dramatically with the OAM mode increasing and the value of the gain for Array 2 is approximately 19.8 dBi, which has fallen greater than 6 dB when Array 2 ($l = 1$) is compared with Array 1 ($l = 0$). Furthermore, the gain shows a substantial reduction with the increase of the mode when Array 4 ($l = 2$) is compared with Array 2 ($l = 1$).

Moreover, the gains will also be dropped by approximately 2 or 3 dB after 1-bit phase quantization comparing Array 2 with Array 3 or Array 4 with Array 5. That is to say, 1-bit phase quantization probably leads to a reduction of approximately 3 dB in the absence of any change in other conditions.

With the substantial reduction of the gain for Array 5, a simple method to increase the gain is proposed. The number of Array 6 is set to 1,600 elements (40×40) increased by four times, while the gain has a strong improvement by approximately 6 dB, which is similar to our experience with the array antenna.

This results mentioned above are also in line with common sense, as OAM beams lead to a significant reduction in gains, and the gain decrease regularly with the value of mode increasing because of the helical phase. While, increasing the number of cells on array is an effective way to improve the gain. In other words, as the number of elements increases, the OAM gain improves as well as that of the traditional array antenna. Therefore, the design of a large-scale array is necessary because it can improve the peck gain from the third column.

2) DIVERGENCE ANGLE OF MAIN LOBE

The divergence angle for different arrays can be obtained by Eq. (5), and the result is the value of theta with a maximum peck gain in 3D space which is represented by θ max as shown in Table 1. While, Θ represents an inverse transformation about the maximum peck gain, moreover the corresponding θ max value can be obtained from the direction of the maximum gain. Furthermore, the severity of pattern splitting can be presented by the divergence angle θ max. In addition, a small value or narrow divergence angle is needed to increase the distance of OAM-based communication.

TABLE 1. Detailed indicators of vortex performance for different OAM beams.

Array (1-6)	Array Parameters			Gain (dBi)	Div. Angle	Det Gain (dBi)	Eff. (%)
	Mode	Phase	Size				
Array1	*l*=0	360°	20×20	27.0	0°	0	40
Array2	*l*=1	360°	20×20	19.8	6°	3.0	7.6
Array3	*l*=1	1-bit	20×20	17.8	6°	3.6	4.8
Array4	*l*=2	360°	20×20	17.5	8°	2.6	4.5
Array5	*l*=2	1-bit	20×20	14.9	8°	3.4	2.5
Array6	*l*=2	1-bit	40×40	21.6	4°	0.9	2.9

A perfect pencil-beam for high gain on Array 1 is presented, however, the OAM beams split, such as Arrays 2, 3, 4, 5 and 6, as represented by the divergence angle of the main lobe in the fourth column in Table 1. The divergence angle of Array 1 is equals to zero; therefore, a high-gain beam is generated and can propagate for a long distance. When the mode of the OAM beam is equals to $l = 1$ for Array 2, the OAM beam is split, and the divergence angle of the main lobe is approximately 6°. The value of the divergence angle is enlarged with the increase of mode, which means that the OAM beams become more divergent comparing Array 4 ($l = 2$) with Array 2 ($l = 1$). In addition, the same conclusion can be obtained comparing Array 5 ($l = 2$) with Array 3 ($l = 1$) by using the 1-bit phase element.

$$\theta_{\max} = \Theta(\max(Gain(\theta, \varphi))) \tag{5}$$

Interestingly, the divergence angle of the main lobe positively correlates with the mode of OAM but has nothing to do with 1-bit phase quantization comparing Array 2 with Array 3 or Array 4 with Array 5.

It is noteworthy that the divergence angle becomes narrow with the increasing of elements number as Array 6. Therefore, the design of large-scale arrays is meaningful for the

convergence of the OAM beam to increase the distance of OAM-based communication links.

3) THE FLUCTUATION GAINS OR CIRCUMFERENTIAL SYMMETRY IN AZIMUTH PLANES

As shown in the first row in Fig. 5, the gains at different azimuth planes for the OAM beam are not equal to each other, which is different from the Array 1 for the high-gain beam. Therefore, the fluctuation gain is investigated as an indispensable indicator for OAM beams for the first time. Furthermore, it is the maximum difference value on the φ-plane with a fixed θ max, and the θ max is the value of the divergence angle mentioned above calculated by Eq. (5). Furtherly, the fluctuation gain (det *Gain*) is equals to the difference value between the maximum gain and the minimum gain in different φ-planes obtained by Eq. (6). The fluctuation gains for different Array are shown in the fifth column in Table 1. The value of Array 1 is equals to zero, that is to say, the peck gains in all azimuth planes are equal to the maximum gain. However, the fluctuation gain is significantly increased approximately 3.0 dB with the mode of $l = 1$ because of the twisted phase distribution in Array 2 compared with Array 1. The fluctuation gains of the OAM beams are approximate equality or some improvements comparing Array 2 with Array 4 and Array 3 with Array 5, which shows that the fluctuation gain is not affected by the OAM mode changing. That is to say, the gain is decreased while the fluctuation gain is not deteriorated with the increasing of OAM mode.

$$\det Gain = \max(Gain(\theta_{\max}, \varphi)) - \min(Gain(\theta_{\max}, \varphi)) \quad \text{While, } \varphi = [0, 2\pi] \tag{6}$$

Moreover, comparing Array 3 with Array 2 after 1-bit phase quantization, we find that the fluctuation gain of OAM beam increases a little approximately 0.6 dB, and only two states of phase exist, 0° or 180° in Array 3. The same phenomenon can be obtained comparing Array 5 with Array 4, in which only phase elements change. Therefore, the fluctuation gains of OAM-carrying beams have not too much changing with the switching of OAM mode from $l = 1$ to $l = 2$ and the 1-bit phase quantization based on the previous analysis, and the values for different OAM beams are the same approximately 3 dB.

It is noteworthy that a large-scale array such as Array 6 for an OAM mode of $l = 2$ lead to a smaller fluctuation gain than Array 5. Therefore, the design of large-scale arrays is feasible for steady gains in all azimuth planes.

4) EFFICIENCY

Ultimately, aperture efficiencies of arrays are presented in the last column in Table 1. According to the simulation results, the efficiency for different arrays decreases with the increasing of OAM mode and the using of 1-bit phase element.

As shown in Table 1, the efficiency for Array 1 with mode of $l = 0$ is acceptable. However, the efficiency deteriorates with the increasing of the OAM mode, comparing Array 2 with Array 4, or Array 3 with Array 5. Meanwhile, the same trend is observed for 1-bit phase quantization in which the efficiency reduces in equal proportion when Array 2 is compared with Array 3 and Array 4 is compared with Array 5, and only the phase element on the proposed metasurface changes. However, un-consistent with the conclusion of the above indicators, large arrays for the OAM beam are not useful in improving efficiency with the increasing of aperture size, which has some minor improvements for it but no too much. The reason for the case of efficiency can be obtained by Eq. (9). As we know, the gain of Array 6 has been improved by increasing the number of array element comparing with Array 5, meanwhile, the size of array *As* has also been increased which will impact the aperture efficiency η. The common measures for furtherly increasing the efficiency are shown as follows: reduce the loss of element, optimize the best height of feed, optimize det-φ, and so on. However, in our design, the feed height and the value of det-φ are both optimal in this reflectarray system. Only the method of improving the element can be used, and it is another category problem which will be presented in future.

Therefore, large arrays are helpful to improve most indicators of OAM beams from the aforementioned analysis, such as the maximum gain, the divergence angle and the fluctuation gains. And this method is simple to realize.

IV. PROTOTYPE TEST OF 1-BIT PROGRAMMABLE METASURFACE

In the previous sections, 1-bit elements with fixed-phase states are used to verify the feasibility of realizing the OAM beam. Through comparative analysis based on several key parameters, the far-field radiation performance for OAM beam are systematically studied. However, the 1-bit phase element mentioned above cannot be used for real time control of electromagnetic waves. To meet the dynamic development demands in future, a reconfigurable reflective element [40] with three layers of substrates is introduced in this section. The first layer is Taconic TLX-8 (dielectric constant 2.55, loss of tangent 0.0019) for radiation with a thickness of 1.58 mm, and other layers are FR4 structure (dielectric constant 4.4, loss of tangent 0.02) for biasing circuits with a thickness of 0.5 mm. Next, a low-cost PIN diode of Skyworks SMP1340 is introduced on each reconfigurable radiation element. Moreover, the PIN diodes can be switched "ON" and "OFF" by supply different bias voltages for the PIN diode as +0.8 V and -12 V, thereby presenting the different phase states of the proposed coding particle with about 180° reflective phase difference and low reflection loss. The center working frequency about reconfigurable reflectarray is at 9.37 GHz, which does not affect the verification of the conclusion mentioned-above. In addition, the proposed PIN diode acts as a model of an inductor *Lon* and a resistor *Ron* in series, under the "ON" state, while under the "OFF" state it can be acted as a resistor *Roff*, an inductor *Loff*, and a capacitance *Coff* in series. Moreover, the extracted parameters for this PIN diode are: *Lon* = 450pH, *Ron* = 1Ω, *Roff* = 10Ω,

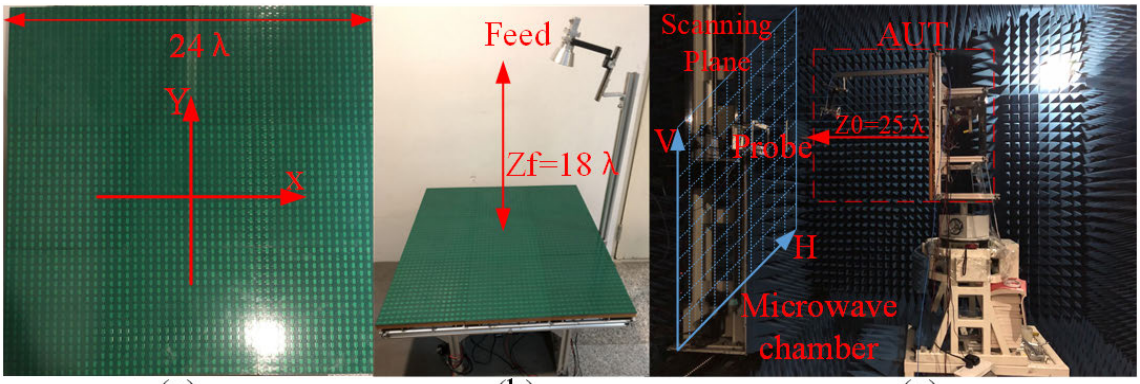

FIGURE 6. Antenna prototype for OAM beam and near-field measurement system: (a) proposed active 1-bit programmable metasurface, (b) antenna prototype, (c) planar near-field scanning microwave chamber.

an inductor $Loff = 450$ pH, and a capacitance $Coff = 100$fF. Then, the detailed structure of this reconfigurable element are optimized in commercially electromagnetic simulation software HFSS.

Next, to verify the desire high performance OAM beam, a 1-bit active large-scale programmable metasurface with 2304 (48 × 48) reconfigurable elements mentioned above is fabricated for excellent OAM beam. The measured results about the near-field and far-field for the proposed 1-bit programmable metasurface are presented in the following. The topological charge of the OAM beam for $l = 1$ is realized, and the high gain beam for $l = 0$ is also measured.

A. FABRICATION OF METASURFACE AND MEASUREMENT

The proposed metasurface antenna is measured in the near-field scanning measurement system as shown in Fig. 6. The proposed surface is exhibited in Fig. 6 (a) with a size of approximately 768 mm × 768 mm. And the reflection phase difference of the two states of phase for the proposed reconfigurable element is approximately 180° working at 9.37 GHz to meet the requirement of 1-bit phase quantization. Next, a standard horn is introduced as the feed with the gain of approximately 20.6 dBi and the feed is set to a vertical polarization. A tailor-made bracket is employed to fix the feed above the 1-bit programmable metasurface as shown in Fig. 6 (b). In addition, the height of the feed position is optimized at 18 λ (with the F/D ratio approximately 0.76) for the best aperture efficiency to obtain outstanding antenna performance. The planar near-field scanning microwave chamber is shown in Fig. 6 (c), and the metasurface antenna is located on the rotary table.

B. MEASURED NEAR-FIELD RESULTS

To measure the magnitude and phase distributions of electric field in the near region for the OAM beam, a near planar scanning method is performed to detect the phase wave-front of the OAM beam as shown in Fig. 6 (c). A standard scanning probe antenna is used to measure the vertical polarization component of the reflected e-field. The sampling plane is placed at the distance of 25 λ away from the proposed 1-bit surface. And the probe scans are conducted from -728 mm to 728 mm in two directions with a sampling period 16 mm.

1) MAGNITUDE AND PHASE DISTRIBUTIONS

The measured magnitude and phase distributions for the vertical component of the e-field are presented in Fig. 7. In Figs. 7 (a) and (b), the amplitude and phase distributions of the vertical component of the e-field for high gain beam are presented by using the proposed 1-bit metasurface. In addition, an excellent isophase plane is realized in Fig. 7(b), and the upper half of the central region causes a certain degree of interference due to the blockage of the feed. Meanwhile, the amplitude and phase distributions for the OAM beam with the mode of $l = 1$ are also shown in Figs. 7 (c) and (d). Notably, a circular-ring-shaped magnitude distribution with a null in the central region is achieved in Fig. 7(c). Furthermore, 360° helical phase distribution is already able to express the generating of the OAM beam by using the 1-bit phase element. Negative OAM modes with different helical directions can also be realized. In addition, a 360° continuously changing phase is produced along the black line in Fig. 7 (d), which can be used to calculate the purity of the OAM spectrum.

2) OAM PURITY

The value of the OAM mode can be obtained from Fig. 7 (d) by counting the number of 360° phase cycles intuitively. However, the purity of the designed mode for OAM beams can be calculated to evaluate the vortex performance. Moreover, to verify the purity of the desired OAM mode, the proportions of the OAM spectrum in each mode are calculated by using the Discrete Fourier transform algorithm in the two working states. From [41], [42], the Fourier relationship between the OAM spectrum $P(\alpha)$ and the corresponding sampling phase $\psi(\varphi)$ can be expressed by Eq. (7-8). In Eq. (7), $\psi(\varphi)$ is the discrete sampling phase along the black circle in the sampling plane, in which the amplitude distributions of the electric field are the largest as shown in Figs. 7 (a) and (c). Therefore, the simulated and measured OAM spectrum is obtained as shown in Fig. 8 through Eq. (7) and (8).

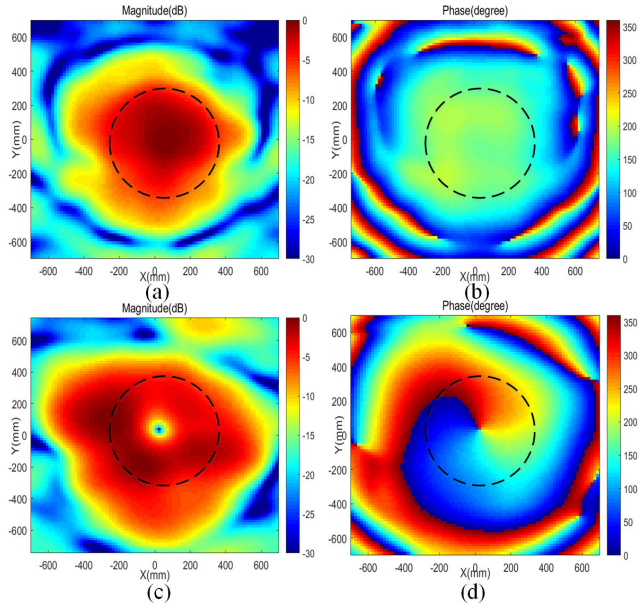

FIGURE 7. Measured magnitude distribution of e-field in near field on XOY plane with distance of 25 wavelengths above the proposed active 1-bit programmable metasurface: (a) mode of $l = 0$ and (c) mode of $l = +1$. Measured phase distribution of e-field in the near field on XOY plane with distance of 25 wavelengths above the proposed active 1-bit programmable metasurface: (b) mode of $l = 0$ and (d) mode of $l = +1$.

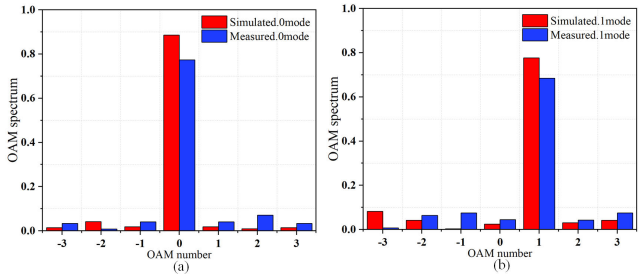

FIGURE 8. Simulated and measured OAM spectrum using the proposed active 1-bit programmable metasurface at 9.37 GHz: (a) mode of $l = 0$ for high-gain beam and (b) mode of $l = 1$ for OAM beam.

Furthermore, the measured proportion for the OAM spectrum with mode of $l = 1$ reaches 68.49% as the simulated one is approximately 77.65%. In addition, in the case of mode of $l = 0$ for high gain, the measured weight reaches 77.39%, corresponding to the simulated result of 88.57%. Evidently, the desired mode occupies most of the weight comparing with other OAM modes.

$$P(\alpha) = \frac{1}{2\pi}\int_0^{2\pi} \psi(\varphi) d\varphi e^{-jl\varphi} \tag{7}$$

$$\psi(\varphi) = \sum_{-\infty}^{+\infty} P(\alpha) e^{jl\varphi} \tag{8}$$

C. MEASURED FAR-FIELD RADIATION PERFORMANCE

The measured far-field normalized radiation patterns are presented in Fig. 9 in 3D view and UV plane for the design of modes $l = 0$ and $l = 1$, respectively.

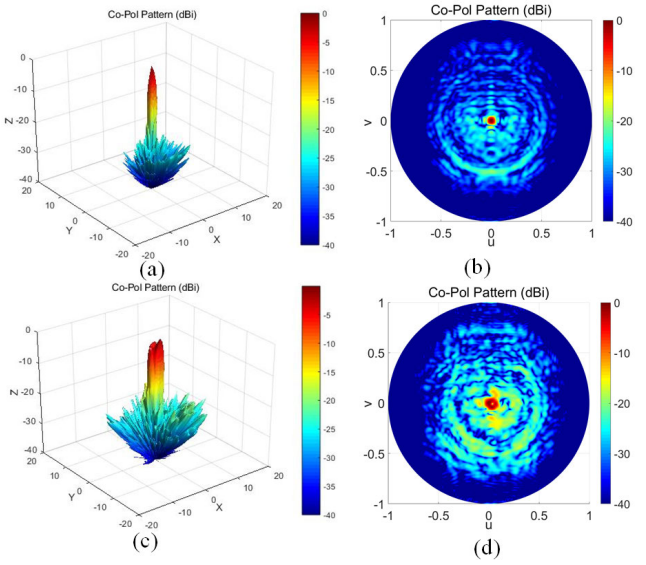

FIGURE 9. Measured radiation patterns for OAM mode of l = 0 and OAM mode of l = 1 by using active 1-bit programmable metasurface: (a) 3D view for mode of $l = 0$, (b) UV plane for mode of $l = 0$, (c) 3D view for mode of $l = 1$ and (d) UV plane for mode of $l = 1$.

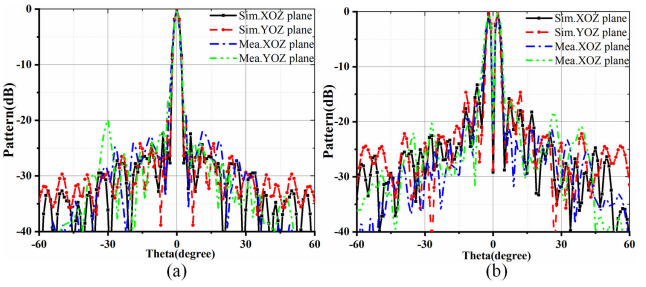

FIGURE 10. Simulated and measured 2D radiation patterns in XOZ and YOZ planes using the proposed active 1-bit programmable metasurface: (a) a high-gain beam with mode of $l = 0$ and (b) an OAM beam with mode of $l = 1$.

Then, the simulated and measured radiation patterns for modes of $l = 0$ and $l = 1$ in the XOZ and YOZ planes are presented in Fig. 10 (a) and (b), respectively. Both the high-gain and OAM beam can be generated. The measured results are in good agreement with the simulated ones. The measured maximum gain for high gain is approximately 31.8 dBi at the direction of positive Z-axis, and the corresponding efficiency is approximately equal to 20.1% computed by Eq. (9). As shown in Eq. (9), the aperture efficiency is proportional to the gain for a specific reflection or transmission array, and the detailed discussed to improve the efficiency has been presented above. Meanwhile, the measured gain of the OAM beam with mode of $l = 1$ is above 26.3 dBi with a drop of 5.5 dB because of OAM beam splitting, and the aperture efficiency is approximately 5.9%. Moreover, the divergence angle of the main lobe improves to approximately 1.8°, which is a small value compared with the conventional reflective or transmissive metasurface [28] for OAM beams; thus, this result benefits the increase of OAM-based communication distance. Furthermore, the measured

fluctuation gain is approximately 0.4 dB, which is also an excellent far-field index for OAM. Therefore, an excellent OAM beam can be generated by using the 1-bit large-scale programmable metasurface in the radio frequency domain. In addition, a high-gain beam with mode of $l = 0$ is obtained, but only the phase distribution on the metasurface needs to be changed.

$$\eta = \frac{G}{4\pi A_s/\lambda^2} \tag{9}$$

D. OAM PERFORMANE COMPARISON

The comparison on other published literatures for OAM beams with this proposed active metasurface are presented in Table 2. The structure of arrays, such as the type of antenna element, feed method, layers of the array and property of the element are investigated. Then, the gains, the divergence angle of main lobe, and OAM modes are presented. Moreover, it is obvious that the structure of the reconfigurable element is simple with a small number of layers. The using of active 1-bit programmable metasurface to obtain OAM beams and the realization of the electromagnetic wave switching between the high-gain beam and OAM beam are rarely discussed. Furthermore, a good performance for the OAM beam with the mode of $l = 1$ is realized with a high gain of OAM approximately 26.3 dBi, which is significantly higher than other published antennas; and an extraordinary small divergence angle of the main lobe approximately 1.8° is achieved, which may be conducive to increase the distance of OAM-based communication in future.

TABLE 2. Comparison with other OAM-carrying antennas in the literature.

Ref.	Array structure				Gain (dBi)	Main Lobe (°)	OAM Mode
	Type	Feed	Layer	Reconfigurable			
18	4MP	Net.	3	No	5.3	30	+1/−1
25	RA	Spa.	2	No	-	-	+2
26	FSS	Spa.	2	No(360°)	-	-	+1/−1
27	HMS	Pro.	2	No	-	-	+1
28	TA	Spa.	4	No(360°)	14.5	9	+1
29	TA	Wav.	5	No(360°)	21.5	5	+1
this	PMS	Spa.	2	Yes (1-bit)	31.8/ 26.3	1.8	0/+1

Notes: Ref. is the abbreviation of reference; Net. is the abbreviation of Network; Spa. is the abbreviation of Space; Pro. is the abbreviation of Probe; Wav. is the abbreviation of Waveguide. Microstrip patch antenna (MP), reflective metasurface antenna (RA), frequency selective surface (FSS), holographic metasurface (HMS), transmission metasurface antenna (TA) and programmable metasurface (PMS).

V. CONCLUSION

In this paper, design, analysis and experiment of a high-performance OAM beam by using a 1-bit programmable metasurface are presented. First, the necessity and feasibility of the realization of the OAM beam based on the 1-bit phase modulation element are studied. Then, a qualitative analysis is conducted in detailed based on key parameters such as element phase quantization, mode of OAM and number of array elements on the OAM performance. Thereafter, a systematic summary and quantitative analysis of the OAM performance are implemented, for instance, the gain, the divergence angle of main lobe and the fluctuation gain. Next, based on the aforementioned conclusions, a large-scale active 1-bit surface is utilized to realize an excellent performance OAM beam with the mode of $l = 1$. By which a high gain of 26.3 dBi is realized with a narrow divergence angle of the main lobe approximately 1.8°, and the fluctuation gain for the OAM beam is approximately 0.4 dB. In other words, this technical index for the OAM beam is incomparable with those reported in the same category of OAM. Moreover, the electromagnetic wave switching from the high-gain plane wave to the vortex wave with the mode of $l = 1$ is achieved and vice versa. Therefore, it lays a foundation for the real time dynamic control of the OAM beam in future. In addition, the reconfigurable technology for the OAM beam has strong portability and it can be extended to millimeter wave, terahertz and optical devices.

ACKNOWLEDGMENT

No conflict of interest exits in the submission of this manuscript, all authors have seen the manuscript and approved to submit to your journal. Thanks to Professor Yang very much for my careful cultivation during my post-doctoral period.

REFERENCES

[1] L. Allen, M. W. Beijersbergen, R. J. C. Spreeuw, and J. P. Woerdman, "Orbital angular momentum of light and transformation of Laguerre Gaussian laser modes," *Phys. Rev. A, Gen. Phys.*, vol. 45, no. 11, pp. 8185–8189, 1992.

[2] S. Franke-Arnold, L. Allen, and M. Padgett, "Advances in optical angular momentum," *Laser Photon. Rev.*, vol. 2, no. 4, pp. 299–313, 2010.

[3] Z. Dutton and J. Ruostekoski, "Transfer and storage of vortex states in light and matter waves," *Phys. Rev. Lett.*, vol. 93, no. 19, Nov. 2004, Art. no. 193602.

[4] S. S. R. Oemrawsingh, X. Ma, D. Voigt, A. Aiello, E. R. Eliel, G. W. 't Hooft, and J. P. Woerdman, "Experimental demonstration of fractional orbital angular momentum entanglement of two photons," *Phys. Rev. Lett.*, vol. 95, no. 24, Dec. 2005, Art. no. 240501.

[5] R. Fickler, R. Lapkiewicz, W. N. Plick, and M. Krenn, "Quantum entanglement of very high angular momenta," *Science*, vol. 338, no. 6107, pp. 640–647, 2012.

[6] S. Bretschneider, C. Eggeling, and S. W. Hell, "Breaking the diffraction barrier in fluorescence microscopy by optical shelving," *Phys. Rev. Lett.*, vol. 98, no. 21, May 2007, Art. no. 218103.

[7] G. Gibson, J. Courtial, M. J. Padgett, M. Vasnetsov, V. Pas'ko, S. M. Barnett, and S. Franke-Arnold, "Free-space information transfer using light beams carrying orbital angular momentum," *Opt. Exp.*, vol. 12, no. 22, pp. 5448–5456, 2004.

[8] B. Thidé, H. Then, J. Sjöholm, K. Palmer, J. Bergman, T. D. Carozzi, Y. N. Istomin, N. H. Ibragimov, and R. Khamitova, "Utilization of photon orbital angular momentum in the low-frequency radio domain," *Phys. Rev. Lett.*, vol. 99, no. 8, Aug. 2007, Art. no. 087701.

[9] J. Wang, J.-Y. Yang, I. M. Fazal, N. Ahmed, Y. Yan, H. Huang, Y. Ren, Y. Yue, S. Dolinar, M. Tur, and A. E. Willner, "Terabit free-space data transmission employing orbital angular momentum multiplexing," *Nature Photon.*, vol. 6, no. 7, pp. 488–496, Jul. 2012.

[10] Z.-G. Guo and G.-M. Yang, "Radial uniform circular antenna array for dual-mode OAM communication," *IEEE Antennas Wireless Propag. Lett.*, vol. 16, pp. 404–407, 2017.
[11] R. Niemiec, C. Brousseau, K. Mahdjoubi, O. Emile, and A. Menard, "Characterization of an OAM flat-plate antenna in the millimeter frequency band," *IEEE Antennas Wireless Propag. Lett.*, vol. 13, pp. 1011–1014, 2014.
[12] D. Jing and W. Jian, "Dielectric metasurfaces enabling twisted light generation/detection/(de)multiplexing for data information transfer," *Opt. Exp.*, vol. 26, no. 10, pp. 13183–13187, 2018.
[13] C. Zhang and L. Ma, "Millimetre wave with rotational orbital angular momentum," *Sci. Rep.*, vol. 6, no. 1, p. 31921, Sep. 2016.
[14] X. Hui, S. Zheng, Y. Hu, C. Xu, X. Jin, H. Chi, and X. Zhang, "Ultralow reflectivity spiral phase plate for generation of millimeter-wave OAM beam," *IEEE Antennas Wireless Propag. Lett.*, vol. 14, pp. 966–969, 2015.
[15] E. Mari, F. Spinello, M. Oldoni, R. A. Ravanelli, F. Romanato, and G. Parisi, "Near-field experimental verification of separation of OAM channels," *IEEE Antennas Wireless Propag. Lett.*, vol. 14, pp. 556–558, 2015.
[16] W. Zhang, S. Zheng, X. Hui, Y. Chen, X. Jin, H. Chi, and X. Zhang, "Four-OAM-Mode antenna with traveling-wave ring-slot structure," *IEEE Antennas Wireless Propag. Lett.*, vol. 16, pp. 194–197, 2017.
[17] Q. Bai, A. Tennant, and B. Allen, "Experimental circular phased array for generating OAM radio beams," *Electron. Lett.*, vol. 50, no. 20, pp. 1414–1415, Sep. 2014.
[18] Q. Liu, Z. N. Chen, Y. Liu, F. Li, Y. Chen, and Z. Mo, "Circular polarization and mode reconfigurable wideband orbital angular momentum patch array antenna," *IEEE Trans. Antennas Propag.*, vol. 66, no. 4, pp. 1796–1804, Apr. 2018.
[19] M. Lin, Y. Gao, P. Liu, and J. Liu, "Theoretical analyses and design of circular array to generate orbital angular momentum," *IEEE Trans. Antennas Propag.*, vol. 65, no. 7, pp. 3510–3519, Jul. 2017.
[20] R. Deng, S. Xu, F. Yang, and M. Li, "An FSS-backed Ku/Ka quad-band reflectarray antenna for satellite communications," *IEEE Trans. Antennas Propag.*, vol. 66, no. 8, pp. 4353–4358, Aug. 2018.
[21] F. Yang, R. Deng, S. Xu, and M. Li, "Design and experiment of a near-zero-thickness high-gain transmit-reflect-array antenna using anisotropic metasurface," *IEEE Trans. Antennas Propag.*, vol. 66, no. 6, pp. 2853–2861, Jun. 2018.
[22] H. Luyen, Z. Yang, M. Gao, J. H. Booske, and N. Behdad, "A wideband, single-layer reflectarray exploiting a polarization rotating unit cell," *IEEE Trans. Antennas Propag.*, vol. 67, no. 2, pp. 872–883, Feb. 2019.
[23] F. Qin, S. S. Gao, Q. Luo, C.-X. Mao, C. Gu, G. Wei, J. Xu, J. Li, C. Wu, K. Zheng, and S. Zheng, "A simple low-cost shared-aperture dual-band dual-polarized high-gain antenna for synthetic aperture radars," *IEEE Trans. Antennas Propag.*, vol. 64, no. 7, pp. 2914–2922, Jul. 2016.
[24] H. Yang, F. Yang, S. Xu, Y. Mao, M. Li, X. Cao, and J. Gao, "A 1-Bit 10×10 reconfigurable reflectarray antenna: Design, optimization, and experiment," *IEEE Trans. Antennas Propag.*, vol. 64, no. 6, pp. 2246–2254, Jun. 2016.
[25] S. Yu, L. Li, G. Shi, C. Zhu, X. Zhou, and Y. Shi, "Design, fabrication, and measurement of reflective metasurface for orbital angular momentum vortex wave in radio frequency domain," *Appl. Phys. Lett.*, vol. 108, no. 12, Mar. 2016, Art. no. 121903.
[26] J. Yang, C. Zhang, H. F. Ma, J. Zhao, J. Y. Dai, W. Yuan, L. X. Yang, Q. Cheng, and T. J. Cui, "Generation of radio vortex beams with designable polarization using anisotropic frequency selective surface," *Appl. Phys. Lett.*, vol. 112, no. 20, May 2018, Art. no. 203501.
[27] X. S. Meng, J. J. Wu, Z. Wu, L. Yang, and L. Huang, "Design, fabrication, and measurement of an anisotropic holographic metasurface for generating vortex beams carrying orbital angular momentum," *Opt. Lett.*, vol. 44, no. 5, p. 1452, 2019.
[28] F. Qin, L. Wan, L. Li, H. Zhang, G. Wei, and S. Gao, "A transmission metasurface for generating OAM beams," *IEEE Antennas Wireless Propag. Lett.*, vol. 17, no. 10, pp. 1793–1796, Oct. 2018.
[29] Y. Chen, S. Zheng, Y. Li, X. Hui, X. Jin, H. Chi, and X. Zhang, "A flat-lensed spiral phase plate based on phase-shifting surface for generation of millimeter-wave OAM beam," *IEEE Antennas Wireless Propag. Lett.*, vol. 15, pp. 1156–1158, 2016.
[30] L.-H. Gao, Q. Cheng, J. Yang, S.-J. Ma, J. Zhao, S. Liu, H.-B. Chen, Q. He, W.-X. Jiang, H.-F. Ma, Q.-Y. Wen, L.-J. Liang, B.-B. Jin, W.-W. Liu, L. Zhou, J.-Q. Yao, P.-H. Wu, and T.-J. Cui, "Broadband diffusion of terahertz waves by multi-bit coding metasurfaces," *Light, Sci. Appl.*, vol. 4, no. 9, p. e324, 2015.
[31] S. Liu, T. J. Cui, Q. Xu, D. Bao, L. Du, X. Wan, W. X. Tang, C. Ouyang, X. Y. Zhou, H. Yuan, H. F. Ma, W. X. Jiang, J. Han, W. Zhang, and Q. Cheng, "Anisotropic coding metamaterials and their powerful manipulation of differently polarized terahertz waves," *Light, Sci. Appl.*, vol. 5, no. 5, p. 16076, 2016.
[32] S. Liu, T. J. Cui, A. Noor, Z. Tao, H. C. Zhang, G. D. Bai, Y. Yang, and X. Y. Zhou, "Negative reflection and negative surface wave conversion from obliquely incident electromagnetic waves," *Light, Sci. Appl.*, vol. 7, no. 5, p. 18008, 2018.
[33] J. Y. Dai, J. Zhao, Q. Cheng, and T. J. Cui, "Independent control of harmonic amplitudes and phases via a time-domain digital coding metasurface," *Light, Sci. Appl.*, vol. 7, no. 1, pp. 2047–2057, Dec. 2018.
[34] H. Yang, F. Yang, S. Xu, M. Li, X. Cao, and J. Gao, "A 1-bit multipolarization reflectarray element for reconfigurable large-aperture antennas," *IEEE Antennas Wireless Propag. Lett.*, vol. 16, pp. 581–584, 2017.
[35] M. Wang, S. Xu, F. Yang, and M. Li, "Design and measurement of a 1-bit reconfigurable transmitarray with subwavelength H-Shaped coupling slot elements," *IEEE Trans. Antennas Propag.*, vol. 67, no. 5, pp. 3500–3504, May 2019.
[36] H. Yang, F. Yang, X. Cao, S. Xu, J. Gao, X. Chen, M. Li, and T. Li, "A 1600-element dual-frequency electronically reconfigurable reflectarray at X/Ku-band," *IEEE Trans. Antennas Propag.*, vol. 65, no. 6, pp. 3024–3032, Jun. 2017.
[37] Y. Yuan, K. Zhang, B. Ratni, Q. Song, X. Ding, Q. Wu, S. N. Burokur, and P. Genevet, "Independent phase modulation for quadruplex polarization channels enabled by chirality-assisted geometric-phase metasurfaces," *Nature Commun.*, vol. 11, no. 1, pp. 4186–4195, Dec. 2020.
[38] J. Q. Han, L. Li, H. Yi, and Y. Shi, "1-bit digital orbital angular momentum vortex beam generator based on a coding reflective metasurface," *Opt. Mater. Exp.*, vol. 8, no. 11, pp. 3470–3478, 2008.
[39] K. Guo, Q. Zheng, Z. Yin, and Z. Guo, "Generation of mode-reconfigurable and frequency-adjustable OAM beams using dynamic reflective metasurface," *IEEE Access*, vol. 8, pp. 75523–75529, 2020.
[40] X. Pan, F. Yang, S. Xu, and M. Li, "A 10 240-element reconfigurable reflectarray with fast steerable monopulse patterns," *IEEE Trans. Antennas Propag.*, vol. 69, no. 1, pp. 173–181, Jan. 2021.
[41] W. J. Byun, K. S. Kim, B. S. Kim, Y. S. Lee, M. S. Song, H. D. Choi, and Y. H. Cho, "Multiplexed cassegrain reflector antenna for simultaneous generation of three orbital angular momentum (OAM) modes," *Sci. Rep.*, vol. 6, no. 1, pp. 27339–27347, Jun. 2016.
[42] B. Back, M. J. Padgett, and S. Franke-Arnold, "Angular diffraction," *Sci. Rep.*, vol. 10, no. 10, pp. 103013–103017, 2008.

ZIYANG WANG (Member, IEEE) was born in Henan, China, in 1991. He received the Ph.D. degree in electromagnetic wave and microwave technology from Xidian University, Xi'an, China, in 2018. From 2018 to 2020, he was a Postdoctoral Researcher with the Department of Electronic Engineering, Tsinghua University. He is currently working with the Research Institute for Frontier Science, Beihang University, Beijing, China. His research interests include 1-bit element design, phase controlled electromagnetic surface, vortex electromagnetic wave and spatial beamforming design, global optimization algorithm, 5G MIMO antenna, array antenna decoupling, and antenna broadband design.

XIAOTIAN PAN received the B.S. degree from Zhengzhou University, in 2013, and the M.S. degree from Beihang University, in 2016. He is currently pursuing the Ph.D. degree with the Department of Electronic Engineering, Tsinghua University. His current research interests include reconfigurable reflectarray, reconfigurable transmitarray, and the imaging applications.

FAN YANG (Fellow, IEEE) received the B.S. and M.S. degrees from Tsinghua University, Beijing, China, in 1997 and 1999, respectively, and the Ph.D. degree from the University of California at Los Angeles (UCLA), in 2002.

From 1994 to 1999, he was a Research Assistant with the State Key Laboratory of Microwave and Digital Communications, Tsinghua University. From 1999 to 2002, he was a Graduate Student Researcher with the Antenna Laboratory, UCLA. From 2002 to 2004, he was a Postdoctoral Research Engineer and Instructor at the Electrical Engineering Department, UCLA. In 2004, he joined the Electrical Engineering Department, The University of Mississippi, as an Assistant Professor, and was promoted to an Associate Professor in 2009. In 2011, he joined the Electronic Engineering Department, Tsinghua University, as a Professor, and has served as the Director for the Microwave and Antenna Institute since then. He has published over 400 journal articles and conference papers, seven book chapters, and six books titled *Surface Electromagnetics* (Cambridge University Press, 2019), *Reflectarray Antennas: Theory, Designs, and Applications* (IEEE-Wiley, 2018), *Analysis and Design of Transmitarray Antennas* (Morgan & Claypool, 2017), *Scattering Analysis of Periodic Structures Using Finite-Difference Time-Domain Method* (Morgan & Claypool, 2012), *Electromagnetic Band Gap Structures in Antenna Engineering* (Cambridge University Press, 2009), and *Electromagnetics and Antenna Optimization Using Taguchi's Method* (Morgan & Claypool, 2007). His research interests include antennas, surface electromagnetics, computational electromagnetics, and applied electromagnetic systems.

Dr. Yang is a Fellow of ACES and an IEEE APS Distinguished Lecturer from 2018 to 2020. He was a recipient of several prestigious awards and recognitions, including the Young Scientist Award of the 2005 URSI General Assembly and of the 2007 International Symposium on Electromagnetic Theory, the 2008 Junior Faculty Research Award of the University of Mississippi, the 2009 inaugural IEEE Donald G. Dudley Jr. Undergraduate Teaching Award, and the 2011 Recipient of Global Experts Program of China. He was the Technical Program Committee (TPC) Chair of 2014 IEEE International Symposium on Antennas and Propagation and USNC-URSI Radio Science Meeting. He served as an Associate Editor for the IEEE TRANSACTIONS ON ANTENNAS AND PROPAGATION (2010–2013) and the Associate Editor-in-Chief for *Applied Computational Electromagnetics Society (ACES) Journal* (2008–2014).

SHENHENG XU (Member, IEEE) received the B.S. and M.S. degrees from Southeast University, Nanjing, China, in 2001 and 2004, respectively, and the Ph.D. degree in electrical engineering from the University of California at Los Angeles (UCLA), CA, USA, in 2009.

From 2000 to 2004, he was a Research Assistant with the State Key Laboratory of Millimeter Waves, Southeast University. From 2004 to 2011, he was a Graduate Student Researcher and later a Postdoctoral Researcher with the Antenna Research, Analysis, and Measurement Laboratory, UCLA. In 2012, he joined the Department of Electronic Engineering, Tsinghua University, Beijing, China, as an Associate Professor. His research interests include novel designs of high-gain antennas for advanced applications, artificial electromagnetic structures, and electromagnetic and antenna theories.

MAOKUN LI (Member, IEEE) received the B.S. degree in electronic engineering from Tsinghua University, Beijing, China, in 2002, and the M.S. and Ph.D. degrees in electrical engineering from the University of Illinois at Urbana-Champaign, in 2004 and 2007, respectively.

After graduation, he worked as a Senior Research Scientist at Schlumberger-Doll Research, Cambridge, MA, USA. Since 2014, he joined the Department of Electronic Engineering, Tsinghua University. His research interests include fast algorithms in computational electromagnetics and their applications in antenna modeling, electromagnetic compatibility analysis, and inverse problems. He has published one book chapter, 50 journal articles, and 120 conference proceedings, and holds three patent applications. He also serves as an Associate Editor for IEEE JOURNAL ON MULTISCALE AND MULTIPHYSICS COMPUTATIONAL TECHNIQUES, *Applied Computational Electromagnetic Society Journal*, and a Guest Editor for the Special Issue on "Electromagnetic Inverse Problems for Sensing and Imaging" in *IEEE Antennas and Propagation Magazine*. He was also a recipient of the China National 1000 Plan in 2014 and the 2017 IEEE Ulrich L. Rohde Innovative Conference Paper Award.

DONGLIN SU (Senior Member, IEEE) received the B.S., M.S., and Ph.D. degrees in electrical engineering from Beihang University (BUAA), Beijing, China, in 1983, 1986, and 1999, respectively.

In 1986, she joined the Faculty of School of Electronics and Information Engineering, BUAA, where she was first an Assistant, then a Lecturer, and later on an Associate Professor, and is currently a Full Professor. From 1996 to 1998, she was a Visiting Scholar with the Department of Electrical Engineering, University of California at Los Angeles (UCLA), Los Angeles, CA, USA, under the BUAA-UCLA Joint Ph.D. Program. She has authored more than 100 articles and coauthored several books. Her research interests include the numerical methods for microwave and millimeter-wave integrated circuits and systematic electromagnetic compatibility design of various aircrafts.

Dr. Su is a member of the Chinese Academy of Engineering and a Fellow of the Chinese Institute of Electronics. She received the National Science and Technology Advancement Award of China in 2007 and 2012, and the National Technology Invention Award of China in 2018. She is the Chair of the Beijing Chapter of the IEEE Antennas and Propagation Society and the Deputy Chair of the Antennas Society and the Chinese Institute of Electronics.